Characterization of helium bubbles in Si by slow positron beam

2010 J. Phys.: Conf. Ser. 225 012032

(http://iopscience.iop.org/1742-6596/225/1/012032)

Journal of Physics: Conference Series **225** (2010) 012032 doi:10.1088/1742-6596/225/1/012032

Characterization of helium bubbles in Si by slow positron beam

M Maekawa and A Kawasuso
Advanced Science Research Center, Japan Atomic Energy Agency
1233 Watanuki, Takasaki, Gunma, 370-1292, Japan

E-mail: maekawa.masaki@jaea.go.jp

Abstract. High-dose He-ion-implanted Si has been studied by positron annihilation method. As well known, due to post-implantation annealing at 1173 K, the positron lifetime and the Doppler broadening *S* parameter dramatically increased due to the formation of microvoids. Meanwhile, the post-implantation annealing at 573K resulted in a significant decrease in the positron lifetime and an apparent modification of the Doppler broadening spectrum near the momentum region of p=0.01 m_0c. From the first principles calculation, we confirmed the positron trapping at He bubbles formed in large vacancy clusters.

1. Introduction

It is known that well-ordered microvoids (~10nm) are formed in Si by the high-dose He implantation and subsequent heat treatment [1-4]. Such microvoids have been investigated concerning the gettering issues of Si. As the precursor states of microvoids, helium bubbles with comparable sizes to those of microvoids may be formed. However, the details of helium bubble in Si have not yet been clarified.

Positron annihilation spectroscopy (PAS) is a powerful tool to study defects in materials. Using a slow positron beam, a depth profiling of defects with typical depth of several microns is possible. PAS has been applied to low-dose He ion irradiated Si [5, 6]. For the high-dose He implanted Si, the microvoid formation is mainly reported [7]. However, the positron trapping at helium bubbles in Si has not yet been reported. In this study, we attempted to investigate the fundamental aspects of interaction between positrons and irradiation defects and/or the He bubbles in Si induced by the high-dose implantation of He ions.

2. Experimental

Samples used in this study were cut from a phosphorus-doped *n*-type Si wafer with the resistivity of 48~67 Ω cm. The samples were subjected to the He ion implantation with the energy of 50~200 keV to a dose of 1×10^{17} cm^{-2} at room temperature using a 400 keV ion implanter. The implanted region is estimated to be at 0.5~1.5 μm from the surface by the 'TRansport of Ion in Matter' (TRIM) simulation [8]. After the He implantation, the samples were annealed in argon ambient from 373 K to 1173K.

The Doppler broadening of annihilation radiation (DBAR) measurements were carried out as a function of incident positron energy (*E*). The obtained DBAR spectra were characterized by *S* and *W* parameters, which are defined as the peak and tail intensities, respectively. *S* (*W*) parameter tends to increase (decrease) when positrons are trapped at vacancy defects because of the narrowing of DBAR

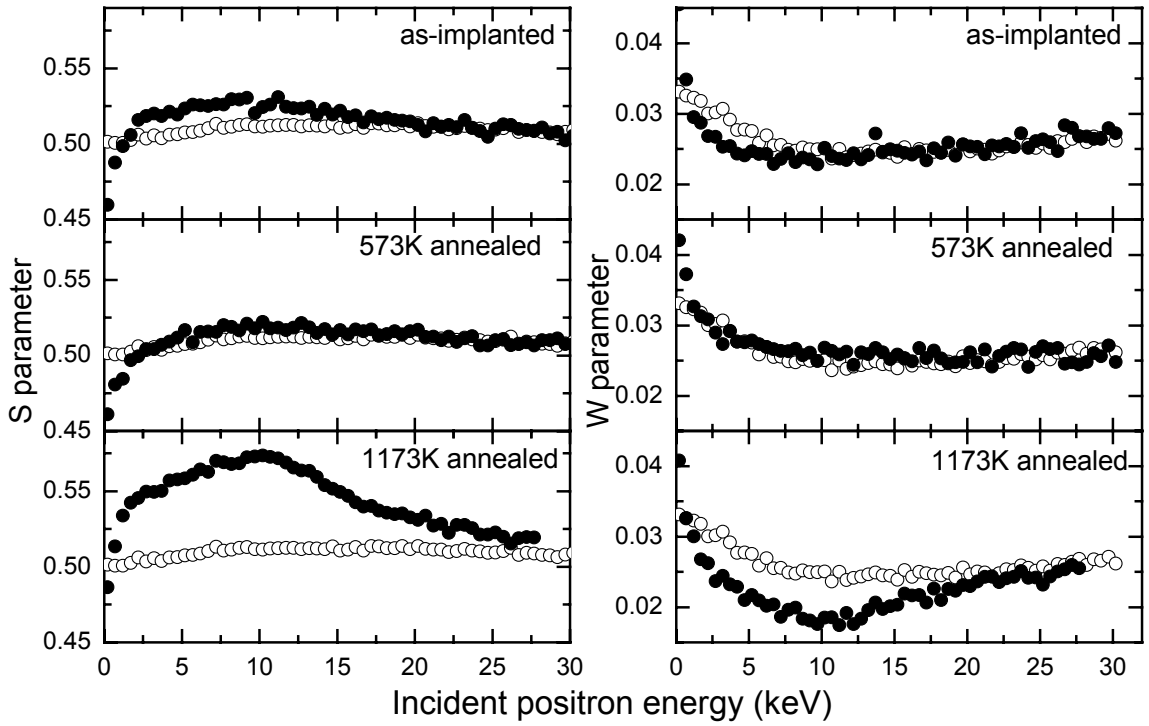

Figure 1. S and W parameters as a function of incident positron energy obtained after annealing at various temperatures. Open circles denote *S* and *W* parameters obtained for the unimplanted state.

spectrum due to the reduction of core electron annihilation rate. All the *S* and *W* parameters are normalized to those for the unimplanted state. To investigate detailed changes in the DBAR spectrum, the coincidence Doppler broadening (CDB) measurement was performed. Positron annihilation lifetime measurements were also carried out using the pulsed positron beam. After subtraction of the background components, the lifetime spectra were analyzed using the PATFIT program [9].

3. Theoretical calculation

To interpret the experimental results, the positron annihilation characteristics were calculated for various model structures based on the first principles manner [10, 11]. The valence electron momentum distribution was calculated using the conventional scheme:

$$\rho_V(\mathbf{p}) = \pi r_e^2 c^2 \sum_n \left| \int e^{-i\mathbf{pr}} \Psi_+(\mathbf{r}) \Psi_n(\mathbf{r}) \sqrt{\gamma(\mathbf{r})} d\mathbf{r} \right|^2, \quad (1)$$

where r_e is the classical electron radius, c is the speed of light, $\Psi_+(\mathbf{r})$ is the positron wave function, $\Psi_n(\mathbf{r})$ is the valence electron wave function of the n-th band, and $\gamma(\mathbf{r})$ is the enhancement factor. The summation was performed over all the occupied states. The core electron momentum distribution was calculated following the Alatalo's method:

$$\rho_C(\mathbf{p}) = \pi r_e^2 c^2 \sum_{i,nlm} \left| \int e^{-i\mathbf{pr}} \Psi_+(\mathbf{r}) \Psi_{i,nlm}(\mathbf{r}-\mathbf{R}_i) \sqrt{\gamma(\mathbf{r})} d\mathbf{r} \right|^2, \quad (2)$$

where $\Psi_{i,nlm}(\mathbf{r}-\mathbf{R}_i)$ represents the core electron wave function specified by the principal, azimuthal, and magnetic quantum numbers (nlm) for the i-th atom and $\mathbf{R}_i$ denotes the position vector. The total momentum distribution is given by $\rho(\mathbf{p})=\rho_V(\mathbf{p})+\rho_C(\mathbf{p})$. The DBAR spectrum was obtained after integrating $\rho(\mathbf{p})$ in two directions and subsequent convolution with the Gaussian resolution function having a FWHM of $3.92\times10^{-3}\,m_0c$. The positron lifetime was obtained by integrating the momentum density in all momentum space.

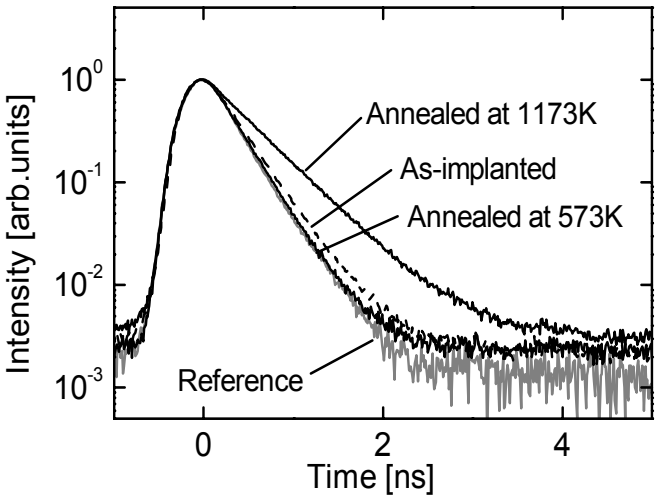

Figure 2. Positron lifetime spectrum for reference, as-implanted state, annealed at 573K and at 1173K.

A supercell with 3×3×3 conventional unit cell containing 216 Si atoms was constructed as a perfect Si crystal. For calculating vacancy states, relevant atoms were removed from this supercell. Also, for He bubbles or He vacancy complexes, the optimum positions of He atoms were determined through the molecular dynamics simulation. The valence electron wavefunctions were calculated based on the norm-conserving pseudo-potential method using the ABINIT4.1.4 code [12]. For the perfect Si crystal, the *k*-point mesh was 2×2×2. The cut-off energy of the plane wave basis set was 24 Ryd. The core electron wavefunctions were represented by the Slater function parameterized by Clementi and Roetti [13]. A self-consistent positron wavefunction was calculated based on the two-component density functional theory in order to minimize the energy functional [14]. The Borónski–Nieminen enhancement factor was adopted.

4. Results and Discussion

Figure 1 shows the *S* and *W* parameters as a function of incident positron energy (*S*-*E* and *W*-*E* curves) obtained after annealing at various temperatures. After the implantation, *S* (*W*) parameters at *E*=5~12 keV corresponding to the He-implanted region increase (decrease) suggesting the introduction of vacancy defects. After annealing at 573 K, *S* (*W*) parameters decrease (increase) to the values for the unimplanted state and subsequently increase (decrease) dramatically with increasing annealing temperature. Figure 2 shows the positron lifetime spectra measured before and after the He implantation and subsequent annealing at 573 K and 1173 K at *E*=8 keV. The prolonged positron lifetime due to implantation is shortened after annealing at 573 K. After annealing at 1173 K, the positron lifetime is sufficiently prolonged.

Detailed annealing behaviour of *S* (*W*) parameters and positron lifetime are plotted in Fig. 3. After annealing at 573 K, *S* parameter decreases to 1.023, while *W* parameter exceeds the level of unimplanted state. Upon the further annealing up to 1173 K, *S* (*W*) parameters reach 1.13 (0.70). The positron lifetime shows similar annealing behaviour to that of *S* parameter. The positron lifetime for the as-implanted state is 270 ps and decreased to 230 ps that is only 10 ps longer than that for the unimplanted state (220 ps). After annealing at 1173 K, the average positron lifetime reaches 500 ps.

It is known that well-ordered microvoids are formed after He implantation and subsequent annealing at 1000-1200 K. The dramatic increases in the *S* parameter and positron lifetime at 1173 K shown in Figs. 1 and 2 are explained as the positron trapping at microvoids as reported in the previous studies [15-17].

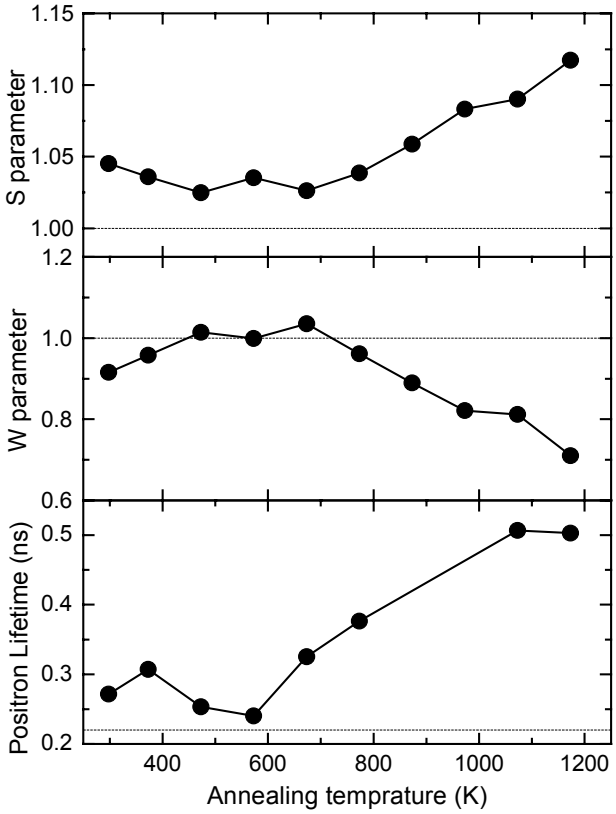

Figure 3. Annealing behaviour of S and W parameters and positron lifetime.

Here, we focus on the decreases in *S* parameter and positron lifetime and the increase in *W* parameter at 573 K. Figure 4 shows the DBAR spectrum measured after annealing at 573 K in the coincidence mode. (To enhance the change of spectrum, the spectrum is differentiated by that of the unimplanted state.) The suppressed intensity in the low momentum region ($0\sim3 \times 10^{-3}$ m_0c) corresponds to the decrease in *S* parameter shown in Figs. 1 and 3. A characteristic bump is seen at around 10×10^{-3} m_0c. This corresponds to the increase in *W* parameter in Figs. 1 and 3. We examine the DBAR spectrum at 573 K and positron lifetime from the aid of the first principles calculation as follows.

Major vacancy defects after the He implantation may be divacancies since monovacancies are mobile at room temperature in Si. It is inferred that due to annealing at 573 K divacancies are occupied by mobile He atoms. Alternatively, He bubbles may be formed as a consequence of He agglomeration. In this case, relatively large open volumes are filled with He atoms. As shown in Fig. 4, by introducing He atoms into divacancies the calculated spectrum becomes to be analogous with the experiment, but the overall spectrum shapes are not compatible. Meanwhile, when a large vacancy cluster (V_{18}) with an approximate diameter of 1 nm is filled with He atoms the experimental spectrum is better explained.

Figure 5 shows the calculated positron lifetimes for divacancy with He atoms and V_{18} cluster with He atoms. The positron lifetime decreases with increasing the number of He atoms. The positron lifetimes for divacancy plus two He atoms and divacancy plus four He atoms are 235 ps and 224 ps, respectively. That for V_{18} plus 36 He atoms is 233 ps. These calculated lifetimes are comparable to the

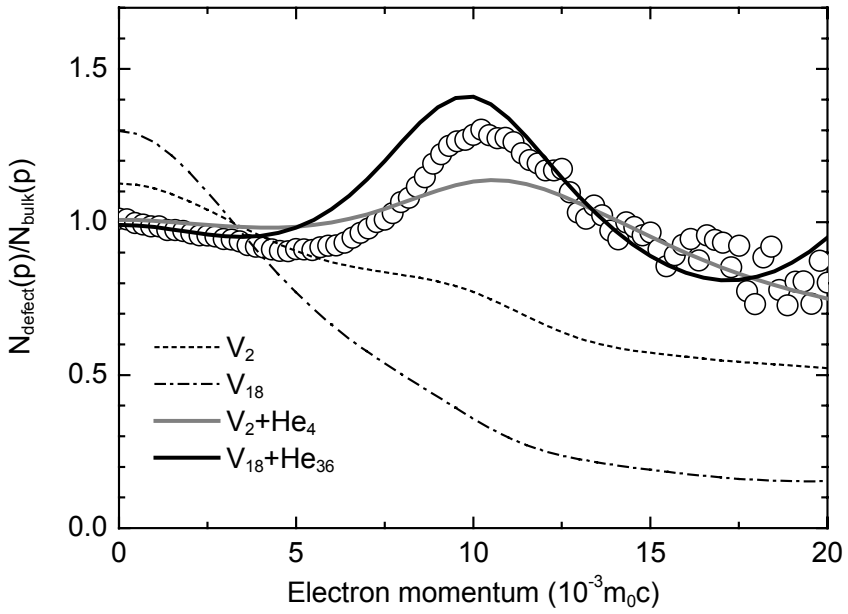

Figure 4. DBAR spectrum obtained after the He-implantation and subsequent annealing at 573 K (open circles) in the coincidence mode. The spectrum is differentiated by that for the unimplanted state to enhance the structure. Calculated DBAR spectra for a divacancy (broken line), a V_{18} cluster (chained line), a divacancy-He_4 complex (gray line) and a V_{18}-He_{36} complex (black solid line) are also shown.

experimental value obtained after the He implantation and subsequent annealing at 573 K as shown in Fig. 3.

The possibility of positron trapping at He bubbles with a few nm radius is also anticipated through a more conventional way as follows: The annihilation rate of positrons (the inverse of lifetime) may be given by

$$\lambda = \pi r_0^2 c Z_{eff} n_{He} + \lambda_{void}, \quad (1)$$

where r_0 is the classical electron radius, n_{He} is the He density in bubbles, λ_{void} is the positron lifetime in empty voids and Z_{eff} is given as 3.94 for He. Having the annihilation rates at 573 K (4.35 ns^{-1}) and 1173 K (2 ns^{-1}) where He bubbles and microvoids are formed, we obtain $n_{He}=8\times10^{22}$ cm^{-3}. This is comparable to that assumed in the above model calculation for V_{18} plus He_{36} ($n_{He}=7\times10^{22}$ cm^{-3}). Combining the gas equation $P=n_{He}kT$, where P is pressure, k is the Boltzmann constant and T is temperature, and the surface tension equation $P=2\gamma/r$ [18], where γ is the surface energy and r is the bubble radius, we obtain

$$r = \frac{2\gamma}{n_{He}kT}. \quad (2)$$

Assuming $\gamma=6.24\times10^{18}$ eV/m^2 for Si [19], the bubble radius is estimated to be approximately 3 nm. Thus, it is concluded that He bubbles with a few nm radius are formed in the low temperature annealing process and positrons are trapped there [6, 20].

Figure 5 shows the cross-sectional transmission electron microscope (TEM) images obtained after the He implantation and subsequent annealing at 573 K and 1173 K. Many small black spots with a few nm radius are observed after annealing at 573 K. After annealing at 1173 K, these black spots vanish and microvoids with 1~40 nm radius appeared. The black spots observed after annealing at 573

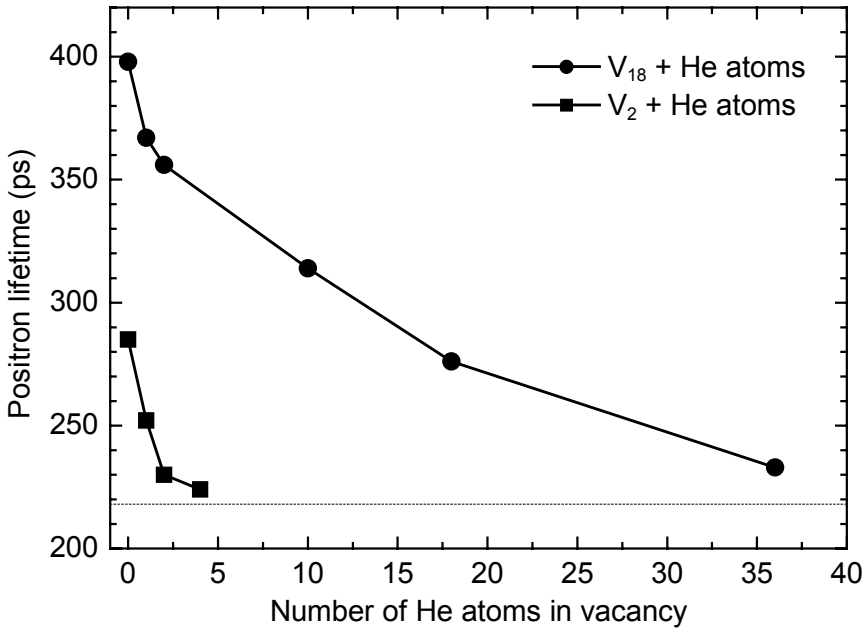

Figure 5. Calculated positron lifetimes for divacancy and V_{18} cluster filled with He atoms as a function of number of He atoms.

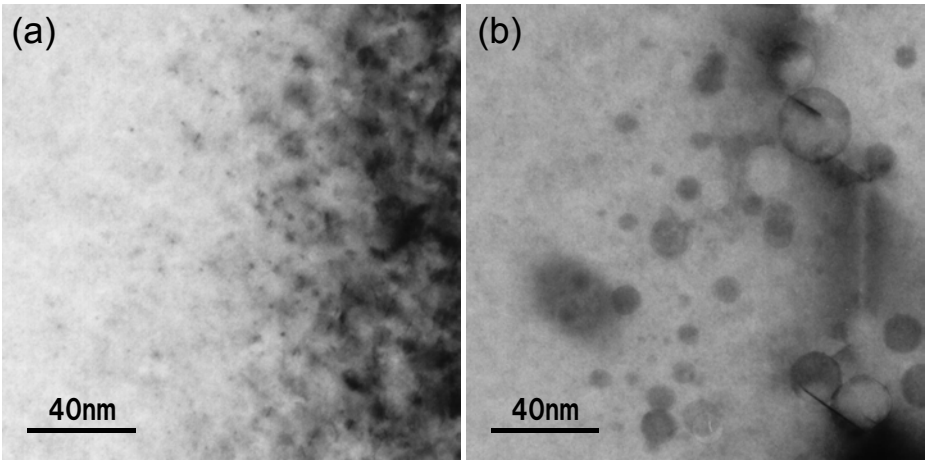

Figure 6. Cross-sectional TEM images obtained after the He implantation and subsequent annealing at (a) 573 K and (b) 1173K.

K probably represent He bubbles where positrons are trapped. During the further annealing process, as a result of coalescence among bubbles and He dissipation, microvoids are developed.

5. Summary

High-dose He-implantated Si has been investigated using positron annihilation spectroscopy. Upon the post-implantation annealing at around 573 K, He bubbles with a few nm size are formed and positrons are trapped there. These He bubbles are probably the source for microvoids formed during the high temperature annealing process up to 1173 K.

References

[1] Griffon C C, Evans J H, De Jong P C, Van Veen A 1987 Nucl. Instr. Methods B **27** 417
[2] Evans J H, Van Veen A and Griffon C C 1987 Nucl. Instr. Methods B **28** 360
[3] Corni F, Nobili C, Ottaviani G, Tonini R, Calzolari G, Cerofolini G F and Queirolo G 1997 Phys. Rev. B **56** 7331
[4] Brusa R S, Karwasz G P, Tiengo N, Zecca A, Corni F, Nobili C, Ottaviani G and Tonini R 1997 Mater. Sci. Forum **255** 665
[5] Brusa R S, Karwasz G P, Tiengo N, Zecca A, Corni F, Tonini R and Ottaviani G 2000 Phys. Rev. B **61** 10154
[6] Corni F, Calzolari G, Frabboni S, Nobili C, Ottaviani G, Tonini R, Cerofolini G F, Leone D and Servidori M 1999 J. Appl. Phys. **85** 1401
[7] Raineri V, Coffa S, Saggio M, Frisina F, Rimini E 1999 Nucl. Instr. Methods B **147** 292
[8] Ziegler J F, Biersack J P and Littmark U, The Stopping and Range of Ions in Solids, 1985, Pergamon, New York
[9] Kirkegaard P, Pederson N, and Eldrup M 1989 Riso-M-**2704**
[10] Puska M J and Nieminen R M 1994 Rev. Mod. Phys. **66** 841
[11] Alatalo M, Barbiellini B, Hakala M, Kauppinen H, Korhonen T, Puska M J, Saarinen K, Hautojärvi P and Nieminen R M 1996 Phys. Rev. B **54** 2397
[12] Gonze X 2002 Comput. Mater. Sci. **25** 478
[13] Clementi E and Roetti C 1974 At. Data Nucl. Data Tables **14** 177
[14] Boroński E and Nieminen R M 1986 Phys. Rev. B **34** 3820
[15] Vishnyakov V M, Donnelly S E, Carter G, Birtcher E C, Haworth L 2002 Solid State Phenomena **82** 267
[16] Krause-Rehberg R and Leipner H S 1998 "Positron annihilation in Semiconductors" Springer
[17] Saito M and Oshiyama A 1996 Phys. Rev. B **53** 7810
[18] Bermond J M, Métois J J, Egéa X and Floret F 1995 Surf. Sci. **330** 48.
[19] Jensen K O, Eldrup M, Singh B N and Victoria M 1988 J. Phys. F **18** 1069
[20] Pivac B, Milat O, Dubek P, Bernstorff S, Corni F, Nobili C, Tonini R 2003 Phys. Status Solidi (a) **198** 29